REGULAR PAPER

Dimensional comparison between amplitude-modulation atomic force microscopy and scanning ion conductance microscopy of biological samples

Japanese Journal of Applied Physics **55**, 08NB18 (2016)
http://doi.org/10.7567/JJAP.55.08NB18

REGULAR PAPER

Dimensional comparison between amplitude-modulation atomic force microscopy and scanning ion conductance microscopy of biological samples

Joonhui Kim[1], MyungHoon Choi[2], Goo-Eun Jung[2], Abdul Rahim Ferhan[1], Nam-Joon Cho[1], and Sang-Joon Cho[2,3*]

[1]*School of Materials Science and Engineering, Nanyang Technological University, Singapore 639798*
[2]*Research and Development Center, Park Systems, Suwon 16229, Korea*
[3]*Advanced Institute of Convergence Technology, Seoul National University, Suwon 16229, Korea*

*E-mail: msjcho@snu.ac.kr

Received January 8, 2016; revised March 12, 2016; accepted April 25, 2016; published online July 15, 2016

The range of scanning probe microscopy (SPM) applications for atomic force microscopy (AFM) is expanding in the biological sciences field, reflecting an increasing demand for tools that can improve our fundamental understanding of the physics behind biological systems. However, the complexity associated with applying SPM techniques in biomedical research hampers the full exploitation of its capabilities. Recently, the development of scanning ion conductance microscopy (SICM) has overcome these limitations and enabled contact-free, high resolution imaging of live biological specimens. In this work, we demonstrate the limitation of AFM for imaging biological samples in liquid due to artifacts arising from AFM tip–sample interaction, and how SICM imaging is able to overcome those limitations with contact-free scanning. We also demonstrate that SICM measurements, when compared to AFM, show better fit to the actual dimensions of the biological samples. Our results highlight the superiority of SICM imaging, enabling it to be widely adopted as a general and versatile research tool for biological studies in the nanoscale.

1. Introduction

For nearly three decades, scanning probe microscopy (SPM) techniques represent some of the most important and commonly used analytical tools in the field of surface science and materials characterization.[1)] In principle, SPM techniques exploit the interaction between a probe and the surface of a sample to map local physical properties. A map of the sample is obtained by scanning the probe across its surface, line by line with a piezoelectric actuator or scanner. The different methods that can be used to control the relative position of the probe to the sample resulted in several variations of SPM. Among various SPM techniques, atomic force microscopy (AFM) has been widely utilized in biological studies since its conception because of its feasibility to be operated in vacuum, air and even liquid [Fig. 1(a)].[1,2)] However, the sharp tips used in AFM easily interacts with the adhesive and soft nature of the biological surface, often causing it to drag and damage soft biological tissues.[3,4)] To overcome these technical difficulties, a particular variation of SPM known as scanning ion conductance microscopy (SICM) was employed. SICM was first developed by Hansma et al. in 1989[5)] before it was widely used for biological applications in Korchev's group.[6–9)] In principle, SICM measurements are based on changes in ion conductance between two electrodes, monitored via a glass nano-pipette.[10–12)] A schematic of a SICM system is shown in Fig. 1(b). The pipette functions as an AFM tip where the monitored ion current signal is modulated by the gap between the sample surface and the tip apex for feedback control of the pipette–sample distance.[13)] The SICM device positions a scanning nano-pipette[7,8)] at a certain distance above the sample (i.e., typically within the tip diameter range)[14)] and follows topographical changes of the sample without making any contact. Over the years, the sensitivity and stability of SICM have improved with the development of various vertical approach methods such as hopping,[15)] backstep,[16,17)] standing approach,[18,19)] and approach-retract-scanning (ARS) methods.[13,20)] The advantage of the vertical approach lies in its ability to decouple lateral and vertical motions of the pipette, thereby minimizing potential tip–sample interactions leading to more accurate dimensional measurements. In the present study, we compare our dimensional measurements of AFM and SICM images to describe AFM artifacts and advantages of SICM imaging technique.

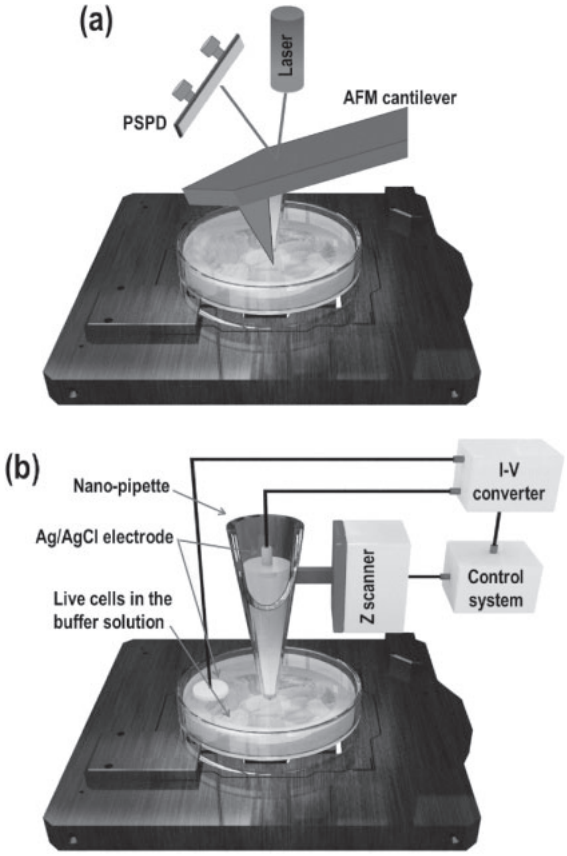

Fig. 1. Schematic representations of AFM and SICM systems. (a) The line indicates the laser pathway from the source, bouncing off the cantilever and into the position sensitive photodiode (PSPD). (b) The figure depicts the nano-pipette, Ag/AgCl electrodes, the current-to-voltage (I–V) convertor, the control system and the piezoelectric z scanner.

2. Materials and methods

2.1 AFM

AFM images were obtained with a commercial SPM (Park Systems XE-Bio System). The setup comprises of an SPM system on the stage of an inverted optical microscope (Nikon TE2000). The SPM system has an *XY* flat scanner ($100 \times 100\,\mu m^2$) and an AFM or SICM head with a 25 μm *z* scanner. All AFM images in this work were taken with amplitude modulation mode both in air and liquid environments. For direct comparison between AFM and SICM, AFM images were taken by raster scanning and ARS method. Raster scanning is a commonly used method in AFM in which the tip is dragged back and forth above the sample surface while maintaining a fixed tip–sample distance. The corresponding ARS method in AFM is known as hopping mode,[21,22] force mapping mode[23] or pulsed force mode.[24] While the force mapping method is usually operated with contact mode AFM, all AFM results reported in this work are obtained using the amplitude modulation technique in order to keep the loading forces as low as possible. The cantilevers used were Olympus Biolever-mini (rectangular cantilever with nominal spring constant of 0.1 N/m and resonance frequency of about 110 kHz) and Nanoworld PNP-TR (triangle cantilever with nominal spring constant of 0.32 N/m and resonance frequency of about 67 kHz) for collagen fibrils and fibroblast cells, respectively. The free oscillation amplitude and setpoint of air dried collagen fibrils were 21 and 7 nm, respectively. Those parameters of collagen immersed in saline were 16 and 10 nm for raster scanning and 12 and 4 nm for ARS with 28 kHz operating frequency, respectively. The fibroblast cell image was taken with 37 nm free oscillation frequency, 2 nm setpoint and 20 kHz operating frequency.

2.2 SICM

SICM images were obtained using the same SPM platform, but with the head exchanged for SICM imaging. SICM Probe, nano-pipettes were pulled from borosilicate capillaries of 1.0 mm outside diameter, 0.58 mm inside diameter (Warner Instruments) using a P-2000 CO_2 laser puller (Sutter Instrument). The fabricated nano-pipette tips have a nominal inner diameter of 100 nm (laser puller pulling parameters: Heat 265, Fil 4, Vel 30, Del 225, Pul 150). An Ag/AgCl electrode, placed in bath solution, was used as a reference electrode for all applied potentials. A separate Ag/AgCl electrode with applied bias was placed inside the nano-pipette tip in order to generate ion current through the tip. For the feedback signal, the ion current was amplified with an analog current-to-voltage converter, as shown in Fig. 1(b). Prior to measurement and imaging, the bias potential at the nano-pipette was set to −150 mV, which roughly corresponded to a current of 0.8 nA. In the present study, images were primarily obtained in the ARS method with a setpoint of 99%.

2.3 Buffer solution

Milli-Q water (resistivity: 18.2 MΩ·cm at 25 °C) was used to prepare all buffer solutions. Phosphate buffered saline (PBS; 10 mM phosphate buffer, 137 mM sodium chloride, and 2.7 mM potassium chloride) was used as the standard electrolyte solution for the SICM measurements. The nano-pipette tip and petri dish used in experiments were also filled with PBS solution.

2.4 Samples

2.4.1 Collagen fibrils. Collagen fibrils were obtained from the tail tendon of Wistar rats and stored in physiological saline with 1–10% tymol (2-isopropyl-5-methylphenol) at 4 °C for a minimum of 1 day. A small piece of the tendon was then stretched on the surface and air dried overnight, followed by immersion of the sample in physiological saline (NaCl) or phosphate buffer saline (PBS) for AFM and/or SICM imaging.

2.4.2 Fibroblast cells. Fibroblast cells were cultured on a petri dish (SPL Lifescience 20035) for 24 h before each experiment in order to promote cell adhesion. It was fixed with 4% formaldehyde for 2 h prior to each experiment, and observed by AFM and SICM.

3. Results

3.1 Imaging collagen fibrils

We compared the capabilities of AFM and SICM to image collagen fibrils. We first prepared air dried collagen fibrils and imaged them using amplitude-modulation AFM with raster scanning (i.e., scanning line-by-line with the AFM tip moving back and forth). It revealed the supercoil structure measuring 140 nm in height and 370 nm in width; the latter taken at 50 nm above the baseline. When the collagen fibril was immersed in saline, it billowed; the height and width increased to 200 and 530 nm, respectively. The use of raster scanning indicated the presence of tip artifact. When the ARS method was employed to minimize lateral artifacts, the width decreased by 100 to 430 nm. Even so, the height-to-width ratio remained at around 1 : 2, indicating the persistence of tip artifacts. In contrast, by using SICM with ARS, the dimensions were 340 and 410 nm in height and width, respectively. It is a good indicator that the height-to-width ratio is close to 1 : 1 because of the supercoil structure of the collagen fibrils and this supports that the SICM measurement of the collagen shows the actual dimensions quite well (Fig. 2). The line profiles of the collagen intersection obtained from AFM and SICM is shown in Fig. 3. A small protrusion, labelled point 1 in Fig. 3(e), appeared subtle in the raster-scanned AFM image, but showed up with clear contrast when imaged using AFM ARS and SICM. In addition, it becomes clear that only SICM is capable of displaying the deformation of the lower collagen from strain of the upper collagen, as indicated by point 2. These results show how each imaging mode could greatly affect dimensional measurement.

3.2 Imaging a cell

Figure 4 demonstrates AFM and SICM images of a fixed fibroblast cell. Unlike collagen fibril, a fibroblast cell showed higher degree of interaction between the AFM tip and the sample surface, even under fixed conditions. It was not feasible to image the cell via raster scanning in AFM due to the abundance of artifacts. Therefore we instead adopted ARS in both AFM and SICM to measure the height pixel by pixel with minimized lateral disturbance. However, even with minimized interactions, stretch marks were still visible in the

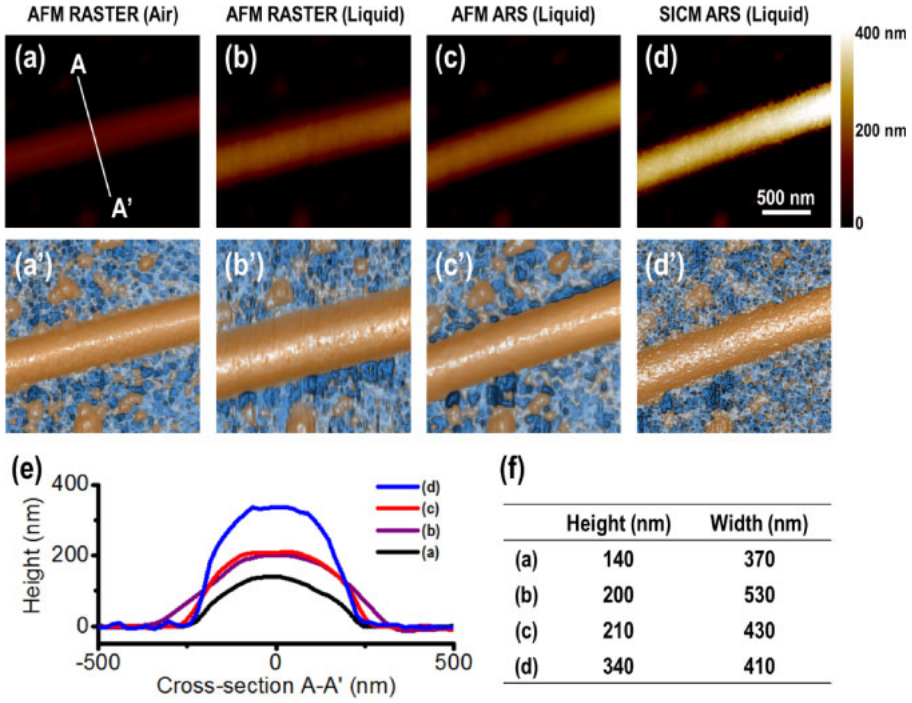

	Height (nm)	Width (nm)
(a)	140	370
(b)	200	530
(c)	210	430
(d)	340	410

Fig. 2. (Color online) A comparison of AFM and SICM capabilities for imaging collagen fibrils. (a) An air dried collagen fibril on a petri dish was first imaged via AFM with raster scanning. The same sample immersed in saline was imaged via (a) AFM with raster scanning, (c) AFM with ARS to minimize lateral artifact, and (d) SICM with ARS. (a′–d′) Edge-enhanced corresponding images in order to show the detailed structure. (e) Height profiles of cross-section A–A′ of each images. (f) Measured height and width values for each profiles.

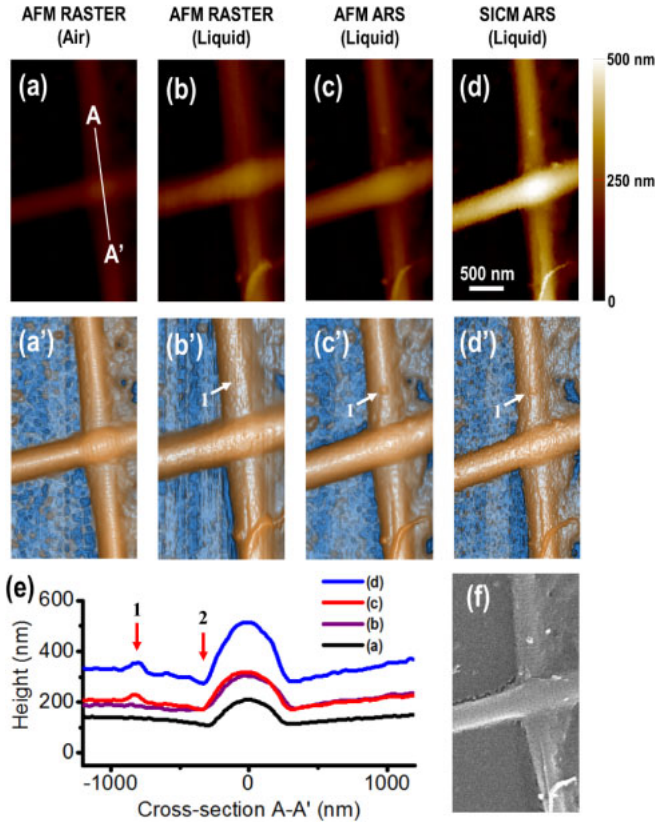

Fig. 3. (Color online) Line profile comparison of AFM and SICM imaging of the collagen intersection. The samples were (a) air-dried, and (b–d) immersed in saline collagen sample. The samples were imaged via (a, b) AFM with raster scanning, (c) AFM with ARS, and (d) SICM with ARS. (a′–d′) Edge-enhanced corresponding images showing the detailed structure. (e) Height profiles of the cross-section A–A′ from the corresponding images. (f) Scanning electron microscopy image of the same collagen fibril.

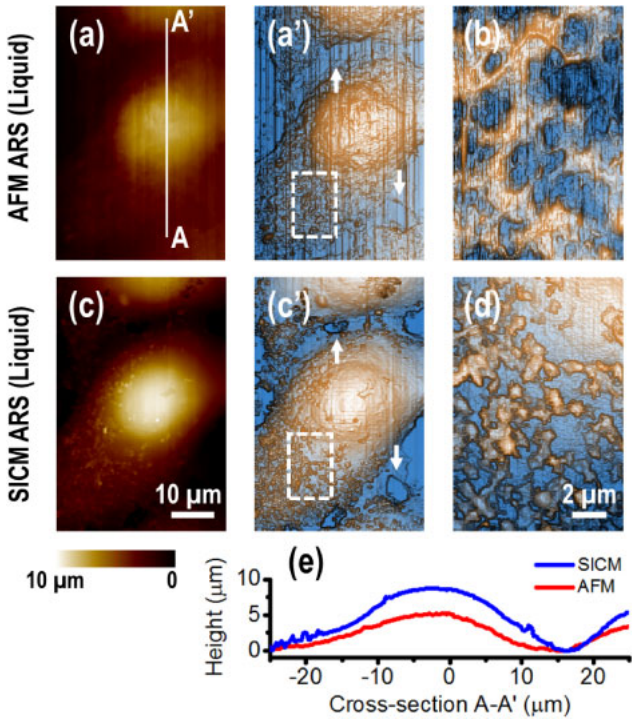

Fig. 4. (Color online) AFM and SICM images of fixed fibroblast. Images in (a), (a′), and (b) were obtained via AFM using the ARS method. The tip–sample interaction artifact manifested as stretch marks in the direction of the raster scan. Images in (c), (c′), and (d) were obtained via SICM using the ARS method. Images in (a′) and (c′) are edge-enhanced. Images in (b) and (d) are edge-enhanced and zoomed in from the corresponding to regions bound by the white dotted boxes in (a′) and (c′), respectively. (e) Line profile comparison of AFM and SICM images along to the line A–A′. The line profile comparison suggested that the downward force applied in AFM is greater than in SICM.

fast scanning direction in AFM. Although ARS did not involve a lateral dragging force, the sample will still be subjected to a vertical downward force of the AFM tip, which can cause deformation especially for soft samples. In addition, outlines of the fibroblast cell was not distinct in AFM images (white arrows in Fig. 4). On the other hand, SICM was able to image the fibroblast three dimensionally without any noticeable artifact, and detailed structures on the cell surface were identifiable when certain areas were zoomed in. Line profile comparison of AFM and SICM images in Fig. 4(e) also shows how the AFM tip could have exerted a downward force on the cell membrane, causing the cell to appear smaller than its actual size. Both AFM and SICM line profiles were processed with the zero height point at the around 16 μm position. The height of the fibroblast obtained in AFM was about 5 μm, which was significantly lower than the SICM measurement of about 9 μm.

4. Discussion

In recent years, the SPM technique has become an increasingly versatile tool in biological sciences, especially in addressing important questions associated with biological surfaces. Indeed, the biological surface/interface supports a wide range of biological processes such as transport, cellular recognition, and signal transduction, to name a few. With the capability to study these structures and their respective functions in a contact-free liquid format with nanoscale resolution, there are many opportunities for the SPM technique to improve upon current measurement capabilities in the biomedical sciences.[25–27)]

The present study compares the capabilities of AFM and SICM for imaging different types of biological samples in a liquid environment. There have been many reports showcasing AFM and SICM images separately, but only few compares the two types of images.[20,28,29)] Moreover, there has been no report comparing amplitude-modulation AFM with the vertical approach method and SICM performed on the same sample. In this paper, we show how different AFM and SICM imaging modes affect the dimensional measurement of the sample. Although there exist plenty of reports involving AFM images used for dimensional measurement of various biological samples, many did not consider artifacts arising from tip–sample interactions. AFM measurement varies quite dramatically upon changes in the bulk and local environment, type of cantilever used, as well as imaging modes. Therefore, in the determination of actual dimensions, AFM tip artifacts have to be considered. Moreover, we found that SICM is suitable for obtaining contact-free images showing the surface topography of biological samples. Furthermore, SICM measurements show minimal deviation from actual dimensions. SICM conducted in ARS mode is especially powerful for imaging samples with steep slopes.[15)] We expected the lateral resolution of ARS mode SICM to be about 150 nm in this paper, depending on the pipette radius.[30)] The resolution of SICM could affect the dimensional measurement but we found that the measurement changes correlate closely with pipette radius (data not shown). The minimized error associated with SICM imaging opens up the possibility of using it as a quantitative tool to measure dimensions of biological samples. While image resolution is still better in AFM than in SICM for some samples, an unchallenged advantage of the latter lies in the ability to obtain images contact-free. As such, SICM is an excellent tool for observing live cells and non-fixed soft samples.

5. Conclusions

Herein, we have demonstrated the superior imaging capabilities of SICM for investigating the dimensional properties of biological examples with contract-free scanning. Indeed, SICM imaging, especially when conducted in ARS mode, is useful for obtaining images that reveal actual three-dimensional topography of biological samples with accurate dimensions. The results indicate that the superior SICM imaging capability enables SICM to become widely adopted as a general and versatile research tool for biological studies in the nanoscale. There are many important applications in the biomedical sciences where a balance between imaging resolution, method of sample preparation, and measurement principle must be achieved in order to effectively probe the surfaces of live biological samples. The imaging capabilities of SICM lend the technique significant potential to achieve this balance, and reveal physiologically relevant insights for clinical diagnosis, molecular toxicology, and pharmaceutical drug development.

Acknowledgements

This work was supported in part by the Advanced Technology Center (ATC) Program (grant number 10045812) and Technology Innovation Program (grant number 10051701) funded by the Ministry of Trade, Industry and Energy to S.-J.C. This work was also supported by the National Research Foundation (NRF-NRFF2011-01), and the National Medical Research Council (NMRC/CBRG/0005/2012) to N.J.C.

1) G. Binnig, C. F. Quate, and C. Gerber, Phys. Rev. Lett. **56**, 930 (1986).
2) H.-J. Butt, E. Wolff, S. Gould, B. D. Northern, C. Peterson, and P. Hansma, J. Struct. Biol. **105**, 54 (1990).
3) E. Henderson, P. Haydon, and D. Sakaguchi, Science **257**, 1944 (1992).
4) H. X. You, J. M. Lau, S. Zhang, and L. Yu, Ultramicroscopy **82**, 297 (2000).
5) P. K. Hansma, B. Drake, O. Marti, S. A. Gould, and C. B. Prater, Science **243**, 641 (1989).
6) Y. E. Korchev, M. Milovanovic, C. L. Bashford, D. C. Bennett, E. V. Sviderskaya, I. Vodyanoy, and M. J. Lab, J. Microsc. **188**, 17 (1997).
7) Y. E. Korchev, C. L. Bashford, M. Milovanovic, I. Vodyanoy, and M. J. Lab, Biophys. J. **73**, 653 (1997).
8) Y. E. Korchev, J. Gorelik, M. J. Lab, E. V. Sviderskaya, C. L. Johnston, C. R. Coombes, I. Vodyanoy, and C. R. W. Edwards, Biophys. J. **78**, 451 (2000).
9) D. Klenerman, Y. E. Korchev, and S. J. Davis, Curr. Opin. Chem. Biol. **15**, 696 (2011).
10) F. Anariba, J. H. Anh, G. E. Jung, N. J. Cho, and S. J. Cho, Mod. Phys. Lett. B **26**, 1130003 (2012).
11) P. Happel, D. Thatenhorst, and I. D. Dietzel, Sensors **12**, 14983 (2012).
12) J. Kim, S.-O. Kim, and N.-J. Cho, Rev. Sci. Instrum. **86**, 023706 (2015).
13) G.-E. Jung, H. Noh, Y. K. Shin, S.-J. Kahng, K. Y. Baik, H.-B. Kim, N.-J. Cho, and S.-J. Cho, Nanoscale **7**, 10989 (2015).
14) M. A. Edwards, C. G. Williams, A. L. Whitworth, and P. R. Unwin, Anal. Chem. **81**, 4482 (2009).
15) P. Novak, C. Li, A. I. Shevchuk, R. Stepanyan, M. Caldwell, S. Hughes, T. G. Smart, J. Gorelik, V. P. Ostanin, M. J. Lab, G. W. J. Moss, G. I. Frolenkov, D. Klenerman, and Y. E. Korchev, Nat. Methods **6**, 279 (2009).
16) P. Happel, G. Hoffmann, S. A. Mann, and I. D. Dietzel, J. Microsc. **212**, 144 (2003).
17) P. Happel and I. D. Dietzel, J. Nanobiotechnol. **7**, 7 (2009).

18) Y. Takahashi, Y. Murakami, K. Nagamine, H. Shiku, S. Aoyagi, T. Yasukawa, M. Kanzaki, and T. Matsue, Phys. Chem. Chem. Phys. **12**, 10012 (2010).
19) H. Yamada, Electrochim. Acta **136**, 233 (2014).
20) T. Ushiki, M. Nakajima, M. Choi, S.-J. Cho, and F. Iwata, Micron **43**, 1390 (2012).
21) H. Kado, S. i. Yamamoto, K. Yokoyama, T. Tohda, and Y. Umetani, J. Appl. Phys. **74**, 4354 (1993).
22) S. Hosaka, T. Morimoto, H. Kuroda, Y. Minomoto, Y. Kembo, and H. Koyabu, Appl. Surf. Sci. **188**, 467 (2002).
23) M. Radmacher, J. P. Cleveland, M. Fritz, H. G. Hansma, and P. K. Hansma, Biophys. J. **66**, 2159 (1994).
24) A. Rosa-Zeiser, E. Weilandt, S. Hild, and O. Marti, Meas. Sci. Technol. **8**, 1333 (1997).
25) Y. Mizutani, M.-H. Choi, S.-J. Cho, and T. Okajima, Appl. Phys. Lett. **102**, 173703 (2013).
26) Y.-Y. Yoo, G.-E. Jung, H.-M. Kwon, K.-H. Bae, S.-J. Cho, and K.-S. Soh, J. Acupunct. Meridian Stud. **8**, 281 (2015).
27) A. Tanaka, R. Tanaka, N. Kasai, S. Tsukada, T. Okajima, and K. Sumitomo, J. Struct. Biol. **191**, 32 (2015).
28) J. Rheinlaender, N. A. Geisse, R. Proksch, and T. E. Schaffer, Langmuir **27**, 697 (2011).
29) J. Seifert, J. Rheinlaender, P. Novak, Y. E. Korchev, and T. E. Schäffer, Langmuir **31**, 6807 (2015).
30) J. Rheinlaender and T. E. Schaffer, Anal. Chem. **87**, 7117 (2015).